

Dynamical characterization of Z_2 Floquet topological phases via quantum quenches

Lin Zhang^{1,*}

¹*ICFO-Institut de Ciències Fòniques, The Barcelona Institute of Science and Technology, Av. Carl Friedrich Gauss 3, 08860 Castelldefels (Barcelona), Spain*

The complete characterization of a generic d -dimensional Floquet topological phase is usually hard for the requirement of information about the micromotion throughout the entire driving period. In a recent work [L. Zhang *et al.*, Phys. Rev. Lett. **125**, 183001 (2020)], an experimentally feasible dynamical detection scheme was proposed to characterize the integer Floquet topological phases using quantum quenches. However, this theory is still far away from completion, especially for free-fermion Floquet topological phases, where the states can also be characterized by Z_2 invariants. Here we develop the first full and unified dynamical characterization theory for the Z_2 Floquet topological phases of different dimensionality and tenfold-way symmetry classes by quenching the system from a trivial and static initial state to the Floquet topological regime through suddenly changing the parameters and turning on the periodic driving. By measuring the minimal information of Floquet bands via the stroboscopic time-averaged spin polarizations, we show that the topological spin texture patterns emerging on certain discrete momenta of Brillouin zone called the 0 or π gap highest-order band-inversion surfaces provide a measurable dynamical Z_2 Floquet invariant, which uniquely determines the Floquet boundary modes in the corresponding quasienergy gap and characterizes the Z_2 Floquet topology. The applications of our theory are illustrated via one- and two-dimensional models that are accessible in current quantum simulation experiments. Our work provides a highly feasible way to detect the Z_2 Floquet topology and completes the dynamical characterization for the full tenfold classes of Floquet topological phases, which shall advance the research in theory and experiments.

I. INTRODUCTION

The discovery of topological quantum states [1–3] has revolutionized the classification of fundamental phases of quantum matter. One of the most famous examples is the integer quantum Hall effect in a two-dimensional (2D) electron gas [4], where the Hall conductance is quantized and is proportional to the Thouless-Kohmoto-Nightingale-den Nijs (TKNN) number [5], a topological invariant that depends only on the global property of the equilibrium ground state. This is sharply distinct from the celebrated Landau-Ginzburg-Wilson framework [6], where the quantum phases are classified by symmetry breaking and are characterized by local order parameters. The studies of topological quantum phases have further become a mainstream of research in condensed matter physics since the discovery of topological insulators [7–10], and a full classification of free-fermion topological systems has been achieved through the tenfold way periodic table [11–14], where each topological phase is either characterized by an integer invariant or by a Z_2 topological index. The most salient and ubiquitous feature of these states is the so-called bulk-boundary correspondence, which states that a system with nontrivial bulk topology shall host protected gapless modes at the boundary [15–17]. This correspondence is the foundation for many experimental detection schemes in quantum materials, such as the transport measurement [10, 18, 19] and angle resolved photoemission spectroscopy [20–22].

Not only restricted in equilibrium systems, the notion of topological phases has also been proposed and realized in Floquet systems [23–35], where the periodic driving provides a versatile approach to create and engineer topological matters [36–47]. Like the static systems, the periodically driven matters can be characterized by quasienergy states with Floquet bands obtained from the effective Floquet Hamiltonian [48, 49]. However, the Floquet topological phases cannot be fully understood via the topological indices from Floquet Hamiltonian due to the additional periodicity in time domain, and anomalous Floquet topological phases have been observed, where the number of edge modes within each bulk band gap is not uniquely determined by the total topological invariants of Floquet bands below this gap [25, 27, 50]. To characterize the Floquet topological phases, new topological invariants involving the micromotion throughout the entire driving period, captured either by the unitary evolution operator [51, 52] (equivalently, we can also consider a set of micromotion-parameterized effective Floquet Hamiltonians [53]) or by the topologically protected singularities in the so-called phase bands [54], have been proposed, which further provide a tenfold way classification of the free-fermion Floquet topological phases [52, 55]. However, it is still challenging to detect a generic Floquet topological state in practical experiments due to the complexity of these invariants.

Recently, considerable efforts have been devoted to detecting topological quantum phases via quench dynamics [56–59] and studying dynamical topological phenomena therein [60–68]. In particular, a dynamical detection scheme was proposed in Ref. [69] and following studies [70, 71] to characterize the Floquet topological phases

* lin.zhang@icfo.eu

using quantum quenches, which is built on the Floquet generalization of the so-called dynamical bulk-surface correspondence for equilibrium topological phases [72–76]. This correspondence shows that the bulk topology of a generic dD system has a universal one-to-one correspondence to the dynamical topological patterns emerging on certain lower-dimensional momentum subspace called (higher-order) band-inversion surfaces (BISs) after quenching the system from a trivial phase to the topological regime, providing the dynamical characterization of topological phases, which can be even generalized to non-Hermitian [77, 78] and higher-order [79–82] topological systems. As the dynamical topological patterns on BISs can be measured directly [83–91], the dynamical characterization scheme of Floquet topological phases proposed in Ref. [69] is highly feasible and has been demonstrated in experiments very recently [92, 93]. Nevertheless, this scheme so far is only applicable to periodically driven systems with integer invariants and is still far away from completion, especially for the free-fermion Floquet topological systems, where the states can also be characterized by Z_2 invariants. Whether a general framework of dynamical characterization theory can be established for these Floquet topological phases is an open question, whose resolution is crucial to advance this research topic and benefits the experimental studies.

In this work, we establish the first full and unified dynamical characterization theory for Z_2 Floquet topological phases of different dimensionality and tenfold-way symmetry classes based on a recent work for equilibrium Z_2 topological phases [76]. By introducing the highest-order BISs in the 0 and π quasienergy gaps, we show that a generic dD Z_2 Floquet topological phase can be characterized by the 0D topological patterns emerging in the stroboscopic time-averaged spin textures after quenching the system from a trivial and static initial state to the topological regime through suddenly changing the parameters and turning on the periodic driving. The dynamical invariants on these two types of BISs uniquely determine the Floquet edge modes in the 0 and π quasienergy gaps, respectively, hence providing a full and feasible dynamical characterization of the Z_2 Floquet topological phases both in the conventional and anomalous sense. We illustrate the applications of this theory via the one- and two-dimensional models. Together with Ref. [69], our work completes the dynamical characterization for the full tenfold classes of Floquet topological phases, which shall advance the research in theory and experiments.

The remaining part of this article is organized as follows. In Sec. II, we first illustrate the characterization scheme via a simple 1D periodically driven model. Then the central result of this work is presented in Sec. III, where we provide the dynamical characterization theory for a generic dD Z_2 Floquet topological phase of the tenfold-way symmetry classes and further show its application in two dimensions. We also discuss the validity and modifications of our theory for driven systems sym-

metric about a generic reference time t_* instead of the trigger time $t = 0$ of quantum quenches in Sec. IV. Finally, the conclusion is provided in Sec. V. More details are shown in the appendices.

II. ILLUSTRATION OF DYNAMICAL CHARACTERIZATION VIA 1D FLOQUET TOPOLOGICAL PHASES

In this section, we start with a simple 1D periodically driven model to illustrate the dynamical characterization scheme. The corresponding Hamiltonian is given by

$$H(k, t) = [\mu(t) - 2t_0 \cos k] \sigma_z + 2\Delta (\sin k \sigma_x + \sin 2k \sigma_y) \quad (1)$$

with the driving $\mu(t) = \mu_0 + \mu_d \cos \omega t$ of period $T = 2\pi/\omega$. Here t_0 is the hopping coefficient, and $\mu_{0,d}$ (or Δ) resembles the Zeeman potential (spin-orbit coupling coefficient). The Pauli matrices are denoted by $\sigma_{x,y,z}$ and are referred to as pseudo spins. To facilitate the discussions, we divide the above Hamiltonian into the static part $H_s = \mathbf{h} \cdot \boldsymbol{\sigma}$ with $\mu_d = 0$ and the periodically driven part $V(t) = \mu_d \cos \omega t \sigma_z$. Due to the particle-hole symmetry $\Xi H(k, t) \Xi^{-1} = -H(-k, t)$ with $\Xi = \sigma_x K$, where K is the complex conjugation operator, the Floquet topological phase (1) belongs to class D and is characterized by Z_2 invariants [52, 54, 55]. Usually, detecting such a phase is quite involved and requires the information in the whole momentum-time space, which is hard to access in practical experiments. To address this issue, here we introduce a highly feasible scheme to characterize the bulk Z_2 Floquet topology based on the higher-order BISs.

A. Band-inversion surfaces for Floquet systems

The concept of (higher-order) BISs was at first proposed to characterize the equilibrium integer topological phases [72, 75], where the n -th order BISs (denoted as n -BISs) are defined as the momentum subspaces with n vanishing Hamiltonian components. Recently, this concept has also been adopted to describe the static Z_2 topological phase by connecting it to a higher-dimensional integer topological phase of the same symmetry class via dimension extension [76], and the BISs for the Z_2 topology are inherited from the corresponding parent integer phase. For the static topological phase H_s without periodic driving, the 0D highest-order 2-BIS [94] exists if $|\mu_0| < 2t_0$ and corresponds to the momenta of Brillouin zone (BZ) with $h_z(k) = 0$, on which the decoupled h_{z} -bands cross with each other while the nonzero field $h_{x,y}$ opens a topological gap and characterizes the static Z_2 topology.

Here we generalize the higher-order BIS characterization into periodically driven Z_2 topological systems. Since the Floquet bands are captured by the Floquet Hamiltonian defined as $H_F \equiv (i/T) \log U(T)$ with $U(t) =$

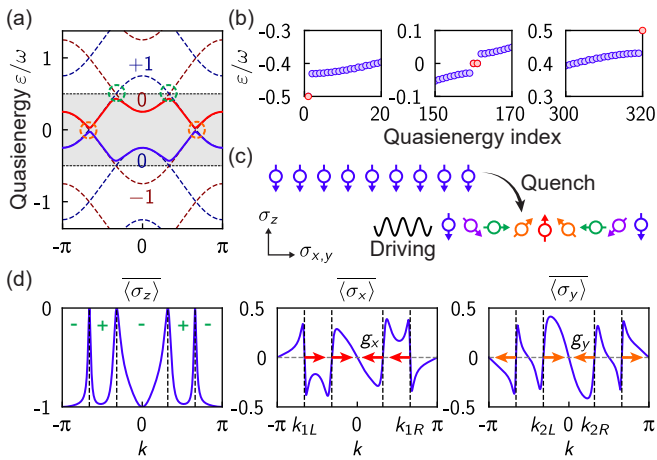


Figure 1. Dynamical scheme to characterize the 1D Z_2 Floquet topological phase. (a) Quasienergy band structure and higher-order BISs. The Floquet bands (solid lines) in the FBZ (shadow region) can be obtained by opening the finite gaps at the crossings of the copied and shifted decoupled h_z -bands labeled by $m = 0, \pm 1, \dots$ (red and blue dashed lines represent $\sigma_z = \pm 1$, respectively) for the cases with weak spin-orbit coupling and periodic driving, which define the 2-BIS points in the 0 (orange dashed circles) or π (green dashed circles) quasienergy gaps. (b) Quasienergy spectrum under open boundary conditions with 160 lattice sites. Both the 0 and π quasienergy gaps support nontrivial edge modes (red dots). (c) Quantum quench protocol. At time $t = 0$, the static initial state fully polarized in the σ_z axis is quenched to the Floquet topological regime by suddenly changing the parameters and turning on the periodic driving. (d) Stroboscopic time-averaged spin textures. The vanishing spin polarizations in all directions determine the 2-BIS₀ points $k_{1L(R)}$ and the 2-BIS _{π} points $k_{2L(R)}$, where the nonzero dynamical fields $g_{x,y}$ are shown in red (or orange) arrows. In the left panel, the regions with $h_{F,z} \geq 0$ are labeled by the symbols “ \pm ”, respectively. Here we set $\mu_0 = 3t_0$, $\mu_d = 3t_0$, $\Delta = 0.2t_0$, and $\omega = 4t_0$.

$\mathcal{T} \exp[-i \int_0^t d\tau H(\tau)]$ and \mathcal{T} denoting the time ordering, which describes the spectra in the Floquet Brillouin zone (FBZ) $[-\pi/T, \pi/T]$ and takes the form of $H_F = \mathbf{h}_F \cdot \boldsymbol{\sigma}$ for time-periodic Hamiltonian (1), we define the 0D highest-order 2-BISs for Floquet systems as 2-BIS $\equiv \{k \in \text{BZ} | h_{F,z}(k) = 0\}$. These BISs can be intuitively understood from the quasienergy operator $Q(t) \equiv H(t) - i\partial_t$ [95], which gives the quasienergy spectra and takes a block-tridiagonal matrix form

$$Q = \begin{pmatrix} \ddots & & & & & & \\ & \tilde{V}^\dagger & H_s + \omega & \tilde{V} & & & \\ & & \tilde{V}^\dagger & H_s & \tilde{V} & & \\ & & & \tilde{V}^\dagger & H_s - \omega & \tilde{V} & \\ & & & & & \ddots & \\ & & & & & & \ddots \end{pmatrix} \quad (2)$$

with $\tilde{V} \equiv (1/T) \int_0^T dt e^{-i\omega t} V(t)$ in the extended Hilbert space $\mathcal{F} = \mathcal{H} \otimes \mathcal{L}_T$, where \mathcal{H} is the physical Hilbert space and \mathcal{L}_T is the space of T -periodic functions with bases

$e^{im\omega t}$ labeled by integer m . In this picture, the Floquet system is considered as a multiband system, where the static Hamiltonian H_s is copied and shifted by energies $m\omega$ ($m = 0, \pm 1, \pm 2, \dots$), leading to the band crossings and giving the BISs; see Fig. 1(a) for an example with weak spin-orbit coupling and periodic driving, for which the Floquet bands can be obtained from the copied and shifted decoupled h_z -bands perturbatively by opening a gap at the band crossings (i.e., BISs) via the off-diagonal blocks \tilde{V} and finite $h_{x,y}$. As the Floquet bands are repeated in the quasienergy domain, it is possible for the Floquet systems to have band crossings both in the center and border of FBZ. For this, we shall divide the BISs into two categories according to the positions of band crossings, i.e., the 0 gap BISs and π gap BISs, and denote them as 2-BIS_{0(π)}, respectively.

To determine which quasienergy gap a BIS belongs to, we first consider the cases with weak spin-orbit coupling and periodic driving. In this case, the 0 and π gap BISs can be identified according to the locations of band crossings for the copied and shifted decoupled bands, as the weak spin-orbit coupling and periodic driving, which open a small gap at these band crossings, will not change their relative positions; see Fig. 1(a). This scheme is also valid for the cases with weak spin-orbit coupling but strong periodic driving. In this case, the static bands in most regions of Brillouin zone resemble the decoupled ones, for which the driving Zeeman field has very limited influence; cf. Eq. (2). Only near the band crossings of original decoupled bands, the spin-orbit coupling mixes different bands and the driving Zeeman field can have remarkable influence on the positions of BISs. As this region is quite small for weak spin-orbit coupling, the above scheme based on decoupled bands still identifies the relative positions of 0 and π gap BISs; see Appendix A 1 for an example.

On the other hand, we also notice that the strong spin-orbit coupling can strongly deforms the decoupled bands and may induce additional BISs; see Appendix A 2 for an example. To identify the 0 and π gap BISs induced by the periodic driving, we can consider the band crossings of the copied and shifted static bands with spin-orbit coupling taken into account, while the 0 gap BISs for the static Hamiltonian and opened by the spin-orbit coupling are still identified by the decoupled bands. We note that for the cases with strong spin-orbit coupling, our characterization theory based on BISs in general only works in the weak periodic driving regime, since the strong spin-orbit coupling mixes the decoupled bands in a large region of Brillouin zone and a strong periodic driving can strongly deforms the static bands, which may cause the coincidence and annihilation of different types of BISs, while leaving the Floquet band topology and edge modes unchanged. However, this limitation will not affect the application of our theory in practical situations, as a strong spin-orbit coupling is not realistic in real experiments.

B. Floquet Z_2 invariant

With these 0 and π gap BISs, we now introduce our Floquet Z_2 invariant. To this end, we note that although the Floquet edge modes cannot be captured by the global topological indices of Floquet bands in the FBZ, it is still possible to utilize the Floquet Hamiltonian to characterize the Floquet topological phases, since the latter contains more information beyond the global band topology. An important type of such information is the local topological structure formed on each BIS, which can uniquely determine the full features of edge modes, as proved in Ref. [70]. It is possible that the global band topology is trivial, while the local topological structures on BISs are still nontrivial. Here we use these local topological structures to characterize the Z_2 Floquet topological phases.

Our Z_2 Floquet invariants defined on BISs are similar to those introduced for the static topological phases in Ref. [76]. But for the Floquet Hamiltonian of periodically driven system (1), we need to define two Z_2 invariants associated with the $q = 0$ and π gap BISs as

$$\nu_q = e^{i\pi(\text{sgn}[h_{F,\alpha}(k_R)] - \text{sgn}[h_{F,\alpha}(k_L)])/2}|_{2\text{-BIS}_q}, \quad (3)$$

where $h_{F,\alpha}$ ($\alpha = x$ or y) should be nonzero on the left (right) point $k_{L(R)}$ of the 2-BIS $_q$ with $h_{F,z}(k) = 0$. Then the Floquet invariant ν_q uniquely determines the edge modes in the corresponding quasienergy gap [Fig. 1(b)], and the Floquet band topology is given by $\nu_0 \cdot \nu_\pi$.

To validate the above statement, we consider the thought experiment proposed in Ref. [51]. Suppose that we start with a system, for which the Floquet bands are all trivial and there is no edge modes in the 0 and π quasienergy gaps. We also assume a weak spin-orbit coupling and periodic driving, such that the local topological structures formed on BISs will not affect each other. As we change the parameters, one of the gaps, e.g., the π quasienergy gap, may close and reopen at certain BISs [i.e., the π gap BISs; see Fig. 1(a)], in such a way that the topological number of Floquet bands becomes nontrivial and there exist edge modes crossing the π quasienergy gap. This case is similar to the static Z_2 topological phases and can be characterized by the Z_2 invariant ν_π defined on the π gap BISs, as proved in Ref. [76].

As the parameters are further varied, the 0 quasienergy gap may close and reopen at other momentum points (i.e., the 0 gap BISs), bringing the Floquet band back to trivial. During this process, the edge modes in the π quasienergy gap cannot disappear, since the π quasienergy gap remains open throughout it. Therefore, after reopening the 0 quasienergy gap, another edge modes must appear around $\varepsilon = 0$. We note that the gap close and reopening at the 0 gap BISs will not affect the local topological structures of π gap BISs for the weak spin-orbit coupling and periodic driving. Hence the characterization of edge modes in the π quasienergy gap via ν_π remains unchanged, while the edge modes in the 0 quasienergy gap is captured by the changes of Floquet

band topology, which is indeed the Z_2 invariant ν_0 defined on the 0 gap BISs, since the summation of these two kinds of BISs gives the total topology of Floquet bands. This demonstrates the validity of our Z_2 Floquet invariant (3) defined on BISs. The above arguments are also valid for the cases with weak (strong) spin-orbit coupling but strong (weak) periodic driving; see Appendix A for examples. On the other hand, as the combination of strong spin-orbit coupling and periodic driving can strongly affect the local topological structures of BISs, our theory may be not applicable in this case. But this will not affect the application of our theory in practical experiments, as clarified before. Without loss of generality, in the following we mainly focus on the cases with weak spin-orbit coupling and periodic driving.

We note that there could be multiple band crossings in each quasienergy gap for certain topological systems, and the above Z_2 invariant can be easily generalized to this situation; see Eq. (8). Moreover, as the BISs can be easily identified from the quantum quenches, our BIS characterization further facilitates the dynamical detection of Z_2 Floquet topological phases, as presented below.

C. Dynamical detection

We consider the quantum dynamics induced by quenching an initially fully polarized state in the σ_z axis with density matrix ρ_0 (i.e., $\mu_0 \gg t_0, \omega$ for the initial state) to the Floquet topological phase (1) at time $t = 0$ through suddenly changing the parameters and turning on the periodic driving [Fig. 1(c)]. The BISs and Floquet topology can be characterized dynamically based on the stroboscopic time-averaged spin textures [69]

$$\overline{\langle \sigma_i(k) \rangle} \equiv \lim_{N \rightarrow \infty} \frac{1}{N} \sum_{n=0}^{N-1} \langle \sigma_i(k, t = nT) \rangle, \quad (4)$$

where $\langle \sigma_i(k, t) \rangle = \text{Tr}[\rho_0(k)U^\dagger(k, t)\sigma_i U(k, t)]$ for $i = x, y, z$ is the spin polarization measured at time t . The numerical results are shown in Fig. 1(d), from which two pairs of momenta with $\overline{\langle \sigma_{x,y,z}(k) \rangle} = 0$ can be identified. Due to $U(nT) = \exp(-iH_F \cdot nT)$, we can readily obtain $\overline{\langle \sigma_i \rangle} = -h_{F,z}h_{F,i}/|\mathbf{h}_F|^2$, which vanishes at the momenta with $h_{F,z}$ or $h_{F,i} = 0$. Thus the above two pairs of momenta indeed measure the 2-BIS $_{0,\pi}$, respectively. The Z_2 Floquet invariant in each quasienergy gap can be further detected through the dynamical field $g_i(k) \equiv -(1/\mathcal{N}_k)\partial_{k_\perp} \overline{\langle \sigma_i(k) \rangle}|_{2\text{-BIS}}$, which quantifies the variation slope of $\overline{\langle \sigma_i \rangle}$ across the 2-BIS and is proportional to $h_{F,i}$ [96]. Here \mathcal{N}_k is a normalization factor and k_\perp denotes the direction pointing from the region $h_{F,z} < 0$ to $h_{F,z} > 0$. As shown in Figs. 1(b) and 1(d), the opposite $g_{x,y}$ on the 2-BIS $_{0,\pi}$ manifests the nontrivial Z_2 Floquet invariant $\nu_0 = \nu_\pi = -1$, consistent with the edge modes in each quasienergy gap.

III. GENERIC DYNAMICAL CHARACTERIZATION SCHEMES

With the above 1D illustration, we now develop in this section the dynamical characterization scheme for a generic dD Z_2 Floquet topological system of the tenfold-way symmetry classes and show its application to a 2D time-reversal invariant Floquet topological model.

A. Generic Z_2 Floquet topological phases

We consider the following periodically driven Hamiltonian in the Altland-Zirnbauer tenfold symmetry classes [52, 55]

$$H[\mathbf{k}; \boldsymbol{\lambda}(t)] = \sum_{i=0}^d h_i[\mathbf{k}; \boldsymbol{\lambda}(t)]\gamma_i + \sum_{i=d+1}^{d'} h_i[\mathbf{k}; \boldsymbol{\lambda}(t)]\gamma_i, \quad (5)$$

which is parameterized by a collection of parameters $\lambda_\ell(t) = \lambda_\ell(t + T)$, such as the driven magnetic field and hopping coefficients. The Clifford algebra γ satisfies $\{\gamma_i, \gamma_j\} = 2\delta_{ij}$ and mimics a (pseudo) spin of dimensionality $n_d = 2^{\lceil d'/2 \rceil}$, where $\lceil \cdot \rceil$ denotes the ceiling function. This model covers all the Z_2 -classified symmetry classes in the tenfold way of different dimensionality [76]. In the absence of periodic driving, the static Hamiltonian $H(\mathbf{k}; \boldsymbol{\lambda})$ with $d' = d+1$ (or $d+2$) describes a dD first (second) descendant Z_2 topological phase [14, 97, 98]. The driven parameters $\boldsymbol{\lambda}(t)$ further bring this system into the interesting Floquet topological regime.

For the Z_2 Floquet topological phases, the symmetries play an important role. Particularly, it has been shown that under the symmetries of Altland-Zirnbauer tenfold classes, the Hamiltonian coefficient is either odd or even with respect to the momentum \mathbf{k} (at most after certain basis change) [76]. Here we assume h_0 to be an even function without loss of generality. With this, we can prove that the periodically driven parameters need to satisfy $\lambda_\ell(t) = \lambda_\ell(-t)$ for the systems with time-reversal symmetry $\Theta H(\mathbf{k}, t)\Theta^{-1} = H(-\mathbf{k}, -t)$ and/or chiral symmetry $\Pi H(\mathbf{k}, t)\Pi^{-1} = -H(\mathbf{k}, -t)$; see Appendix B. This constraint applies to most of the Floquet Z_2 classifications under physical dimensions (i.e., $d = 1, 2, 3$) [52, 55], except for the 1D topological phases of class D, for which the only particle-hole symmetry does not impose any constraint on the driven parameters $\boldsymbol{\lambda}(t)$. On the other hand, for the Floquet systems with synthetic dimensions $d > 3$ [99–101] and only with the particle-hole symmetry, we also assume in this work the above requirement to be satisfied for simplicity, which has covered a broad range of topological states.

B. Dynamical characterization

We now generalize the dynamical characterization theory shown in Sec. II to the generic dD Z_2 Floquet topo-

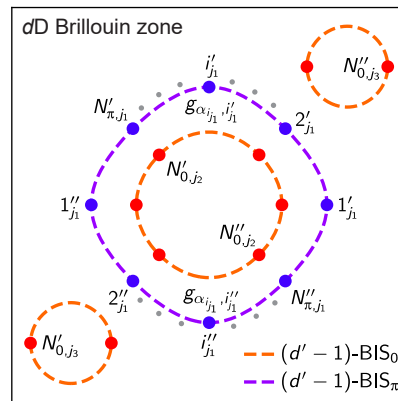


Figure 2. Schematic diagram for the BIS Floquet Z_2 invariant. The higher-order 1D $(d' - 1)$ -BISs are categorized into BISs belonging to the 0 quasienergy gap (orange dashed lines) or the π quasienergy gap (purple dashed line) according to the Floquet band structure. On the j -th $(d' - 1)$ -BIS in the $q = 0$ or π gap, the corresponding 0D d' -BIS points (red or blue dots) are grouped into $N_{q,j}$ symmetric point pairs (i'_j, i''_j) , to each of which a nonzero dynamical field $g_{\alpha_{i_j}} \in \{g_d, \dots, g_{d'}\}$ is assigned, giving the Floquet Z_2 invariant ν_q [see Eq. (8)]. Here the middle rings are single-connected $(d' - 1)$ -BISs with N_{π,j_1} and N_{0,j_2} point pairs, respectively, while the other two circles represent the j_3 -th $(d' - 1)$ -BIS with two disconnected but symmetrically related parts.

logical phase. Similar to the 1D periodically driven system, we consider the quench dynamics starting from an initial state fully polarized in the γ_0 axis. Then the Z_2 Floquet topology can be characterized by the emergent dynamical topology on the highest-order BISs.

For the generic topological phase (5), the Floquet Hamiltonian is given as (see Appendix C)

$$H_F(\mathbf{k}) = \sum_{i=0}^d h_{F,i}(\mathbf{k})\gamma_i + \sum_{i=d+1}^{d'} h_{F,i}(\mathbf{k})\gamma_i. \quad (6)$$

The corresponding higher-order n -BIS $\equiv \{\mathbf{k} | h_{F,i} = 0, i = 0, 1, \dots, n + d - d' - 1\}$ is a $(d' - n)D$ symmetric subspace in the Brillouin zone [76] and can be detected by the stroboscopic time-averaged spin textures $\overline{\langle \gamma_i(\mathbf{k}) \rangle} = -h_{F,0}h_{F,i}/|\mathbf{h}_F|^2$. We first note that the $(d - 1)D$ lowest-order $(d' - d + 1)$ -BIS $^{(i)}$ with only $h_{F,i} = 0$ is determined by the momenta where $\overline{\langle \gamma_\alpha \rangle} = 0$ for all α if $i = 0$ or by the momenta with $\overline{\langle \gamma_i \rangle} = 0$ while not on the $(d' - d + 1)$ -BIS $^{(0)}$ for $i \neq 0$. With these basic BISs, the higher-order BISs can be dynamically constructed as

$$n\text{-BIS} = \bigcap_{i=0}^{n+d-d'-1} (d' - d + 1)\text{-BIS}^{(i)}. \quad (7)$$

Which quasienergy gap the BIS belongs to can be identified as in the 1D case; see Sec. II. Particularly, for the cases with weak spin-orbit coupling and periodic driving, as considered in this work, the 0 and π gap BISs can

also be determined from the Floquet band structure. We would like to mention that the definition of higher-order BISs is actually not unique and the n -BIS can also be defined through any other $(n + d - d')$ Floquet Hamiltonian coefficients and the corresponding $(d' - d + 1)$ -BISs, which does not change the result of dynamical characterization. On the other hand, as which quasienergy gap the higher-order BIS belongs to is determined by the Floquet band structure, which is symmetric with respect to the momentum, the $(d - 1)$ D basic BISs used to construct the higher-order BISs should include those defined by parity even Hamiltonian coefficients, from which the 0 or π gap n -BISs can be most easily identified. This is also necessary for the trivial Z_2 phases with multiple parity even Hamiltonian coefficients. We note that in general, there could be multiple band crossings (i.e., BISs) in each quasienergy gap; see Fig. 2 for an illustration.

To characterize the Z_2 Floquet topology, we further introduce the dynamical field $g_i(\mathbf{k}) = -(1/\mathcal{N}_{\mathbf{k}})\partial_{k_{\perp}}\langle\gamma_i(\mathbf{k})\rangle$ on the 0D highest-order d' -BISs, where k_{\perp} is perpendicular to the $(d' - d + 1)$ -BIS $^{(0)}$ and points to the side with $h_{F,0} > 0$. The dynamical field g_i is proportional to $h_{F,i}$. Then the Floquet topological phases can be fully characterized by the Z_2 invariants defined in the $q = 0$ and π quasienergy gaps and captured by the dynamical topological pattern introduced in Ref. [76]

$$\nu_q = \prod_j \prod_{\substack{i_j \in d'\text{-BISs on the} \\ (d'-1)\text{-BIS}_{q,j}}}^{N_{q,j}} (-1)^{\frac{1}{2}[\text{sgn}(g_{\alpha_{i_j}, i'_j}) + \eta_{q,j} \text{sgn}(g_{\alpha_{i_j}, i''_j})]} \quad (8)$$

with nonzero $g_{\alpha_{i_j}} \in \{g_d, \dots, g_{d'}\}$ of the same parity, which uniquely determines the Floquet boundary modes in the corresponding quasienergy gap. Here the first product is performed over all of the 1D $(d' - 1)$ -th order BISs in the quasienergy gap q , while the second product is performed over the $N_{q,j}$ pairs of d' -BIS points (i'_j, i''_j) located symmetrically on the j -th single-connected $(d' - 1)$ -BIS $_{q,j}$ or the $(d' - 1)$ -BIS $_{q,j}$ with two disconnected but symmetrically related parts (see Fig. 2), for which we have $\eta_{q,j} = (-1)^{N_{q,j}}$ or $\eta_{q,j} = -1$, respectively.

This invariant can be considered as a generalization of Eq. (3) and applies to the cases with multiple BISs and higher dimensions. The corresponding product structure follows the Z_2 nature of the topological phases, for which the combination of a nontrivial band crossing and a trivial one is still nontrivial, while the combination of two trivial or nontrivial band crossings will lead to a trivial phase. On the other hand, as the invariant (8) involves only minimal information about the Floquet system that can be detected in the quantum quench dynamics, it provides a highly feasible scheme to characterize Z_2 Floquet topological phases in real experiments. Particularly, together with the integer Floquet topological phases studied in Ref. [69], the above results further complete the dynamical characterization for the full tenfold classes of Floquet topological phases.

We also note that our dynamical characterization scheme is not affected by the basis change of Hamiltonians, if the resulting Hamiltonian coefficients are still either odd or even with respect to the momentum \mathbf{k} . In this case, the positions of BISs and/or the dynamical fields may be different, but the underlying dynamical Z_2 invariants (8) remain unchanged; see Appendix D for an example. This can be demonstrated from the derivation of BIS Z_2 invariants shown in Ref. [76], where the Z_2 topology is derived from the higher-dimensional integer topological phases by dimension reduction and the dynamical characterization for the latter is unaffected by the basis change [72]. On the other hand, there also exist unitary transformations that can mix the odd and even coefficients. For these situations, our dynamical theory may not work, since the property of the system that the momenta \mathbf{k} and $-\mathbf{k}$ are related by the symmetries will not be reflected on the BISs and in the spin textures, which is important to identify the Z_2 topology. However, this limitation will not affect the application of our theory in practice, as most of the topological systems in experiments possess either odd or even Hamiltonian coefficients (at most after certain basis change).

C. Application to the 2D time-reversal invariant Floquet topological phases

We now utilize the above generic dynamical scheme to characterize the following 2D Floquet topological phase

$$H(\mathbf{k}, t) = \mathbf{h}(\mathbf{k}, t) \cdot \boldsymbol{\gamma} \quad (9)$$

with

$$\begin{aligned} h_0(\mathbf{k}, t) &= m(t) - 2t_0 \cos k_x - 2t_0 \cos k_y \\ &\quad - 2t'_0 \cos(k_x + k_y) - 2t'_0 \cos(k_x - k_y), \\ h_{1,2}(\mathbf{k}) &= 2t_{\text{so}} \sin k_{x,y}, \quad h_{3,4}(\mathbf{k}) = 2t_{\text{so}} \sin(k_x \pm k_y). \end{aligned}$$

Here t_0, t'_0 (or t_{so}) denote the spin-conserved (-flipped) hopping coefficients. Instead of the simple harmonic driving, here we consider the polychromatic square-wave magnetization, given by $m(t) = m_0 + 2m_d/\pi$ (or $m_0 - 2m_d/\pi$) for $-T/4 \leq t < T/4$ (or $T/4 \leq t < 3T/4$), to show the wide validity of our theory. We take $\gamma_0 = \sigma_0 \otimes \tau_z$, $\gamma_1 = \sigma_z \otimes \tau_x$, $\gamma_2 = \sigma_0 \otimes \tau_y$, $\gamma_3 = \sigma_x \otimes \tau_x$, and $\gamma_4 = \sigma_y \otimes \tau_x$, with σ_i and τ_i being Pauli matrices. The 2D Floquet phase (9) possesses the time-reversal symmetry $\Theta H(\mathbf{k}, t) \Theta^{-1} = H(-\mathbf{k}, -t)$ with $\Theta = -i\sigma_y \otimes \tau_0 K$ and belongs to class AII with Z_2 invariant. In Figs. 3(a) and 3(b), we show the quasienergy spectra in the periodic boundary conditions and for a cylindrical geometry with open boundary condition in the y direction, respectively, with $m_0 = t_0$, $m_d = 3t_0$, and $\omega = 7t_0$. There exist protected gapless helical edge modes both in the 0 and π quasienergy gaps.

We study the quench dynamics from a fully polarized initial state in the γ_0 axis by setting $m_0 \gg t_0$ and $\omega = 0$ to the above nontrivial Floquet topological regime. The

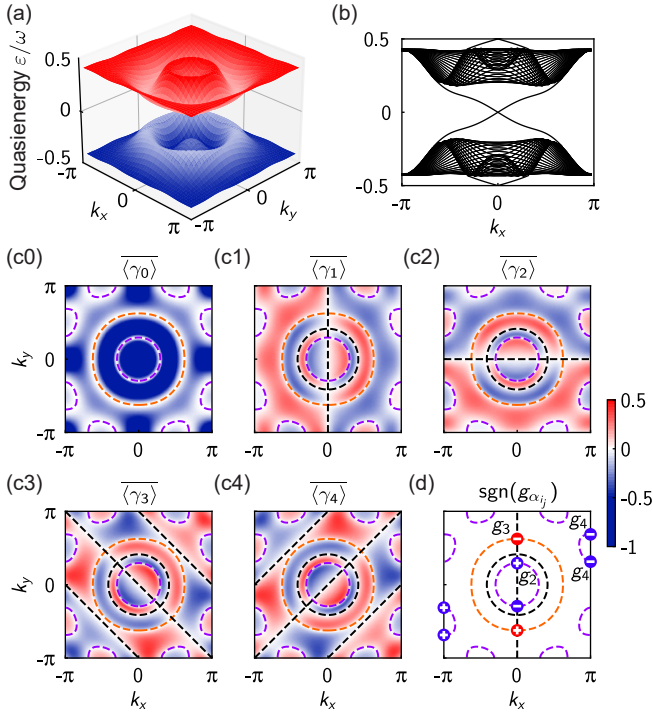


Figure 3. Detecting the 2D time-reversal invariant Floquet topological phase. (a), (b) Quasienergy spectra in the periodic boundary conditions (a) and for a cylindrical geometry with open boundary condition in the y direction (b), where the helical gapless boundary modes on one of the edges in the 0 and π quasienergy gaps are presented. (c0)-(c4) Stroboscopic time-averaged spin textures. Here six ring-shaped structures with $\overline{\langle \gamma_\alpha \rangle} = 0$ for all α emerge, identifying the 1D basic 3-BISs⁽⁰⁾ with vanishing $h_{F,0}$ in the 0 quasienergy gap (orange dashed line) and π quasienergy gap (purple dashed lines), respectively, according to the Floquet band structure (a). Besides, the spin polarization $\overline{\langle \gamma_i \rangle}$ with $i = 1, 2, 3, 4$ also vanishes on the black dashed lines in (c1)-(c4), giving the corresponding 3-BISs⁽ⁱ⁾ with $h_{F,i} = 0$. (d) Dynamical topological pattern. The 0D highest-order 4-BISs (red or blue dots) are constructed as the intersections of 3-BISs⁽⁰⁾ and 3-BISs⁽¹⁾. We assign a nonzero dynamical field $g_{\alpha i_j} \in \{g_2, g_3, g_4\}$ with the sign indicated by “ \pm ” to each symmetric point pair of the 4-BISs, which gives the Floquet Z_2 invariant $\nu_0 = -1$ and $\nu_\pi = -1$. Here we set $m_0 = t_0$, $m_d = 3t_0$, $t'_0 = 0.5t_0$, $t_{so} = 0.5t_0$, and $\omega = 7t_0$.

stroboscopic time-averaged spin textures are shown in Figs. 3(c0)-3(c4), where six ring-shaped structures with vanishing spin polarizations emerge in all the plots of $\overline{\langle \gamma_\alpha \rangle}$ for $\alpha = 0, 1, \dots, 4$, identifying the 1D lowest-order 3-BISs⁽⁰⁾ with $h_{F,0} = 0$. Besides, there are additional lines with $\overline{\langle \gamma_i \rangle} = 0$ for $i \neq 0$ in the corresponding spin texture, capturing the 3-BISs⁽ⁱ⁾ with $h_{F,i} = 0$. In Fig. 3(d), we use 3-BISs⁽⁰⁾ and 3-BISs⁽¹⁾ to construct the 0D highest-order 4-BISs. According to the Floquet band structure [Fig. 3(a)], the 4-BIS points on the outer 3-BIS⁽⁰⁾ that surrounds the $\mathbf{k} = (0, 0)$ point belong to

the 0 quasienergy gap, while the others represent the 4-BISs _{π} . We assign a nonzero dynamical field $g_{\alpha i}$ to each symmetric point pair of these 4-BISs, with which we can obtain the Z_2 invariant $\nu_0 = -1$ and $\nu_\pi = -1$, characterizing the Floquet topological phase.

We would like to mention that the dynamical characterization scheme built on the BISs requires the Floquet bands in the FBZ to be gapped. For the special 2D time-reversal invariant driven system with only two bands as considered in Ref. [54], the bulk Floquet bands are related by the time-reversal symmetry and the corresponding gap necessitates to close at high symmetry momenta, leading to a gapless Floquet Hamiltonian H_F , to which our approach is not applicable.

IV. FLOQUET TOPOLOGICAL SYSTEMS WITH GENERIC REFERENCE TIME

In the above discussions, the periodically driven Hamiltonians are assumed to be symmetric about the trigger time $t = 0$ of the quantum quench dynamics. In this section, we further discuss the dynamical characterization for Floquet topological phases $H(\mathbf{k}, t; t_*)$ that are symmetric about a generic reference time t_* , i.e., $\Theta H(\mathbf{k}, t; t_*) \Theta^{-1} = H(-\mathbf{k}, 2t_* - t; t_*)$ and $\Pi H(\mathbf{k}, t; t_*) \Pi^{-1} = -H(\mathbf{k}, 2t_* - t; t_*)$. As before, we use the notation $H(\mathbf{k}, t)$ for the Floquet Hamiltonian with $t_* = 0$ and have the relation $H(\mathbf{k}, t; t_*) = H(\mathbf{k}, t - t_*)$ for a generic reference time t_* .

A. Direct measurements

We first consider the dynamical characterization scheme proposed above without any modifications. The time evolution operator over one period now reads

$$U(T; t_*) \equiv \mathcal{T} e^{-i \int_0^T d\tau H(\tau; t_*)} = e^{-iH''(T-2t_*)} \cdot e^{-iH' \cdot 2t_*} = e^{-iH_F^{(t_*)} T}, \quad (10)$$

where we have $H' = (i/2t_*) \log U(t_*, -t_*)$ and $H'' = [i/(T - 2t_*)] \log U(T - t_*, t_*)$ with $U(t_f, t_i) \equiv \mathcal{T} \exp[-i \int_{t_i}^{t_f} d\tau H(\tau)]$. Similar to the proof in Appendix C, one can readily show that H' and H'' take the form of Dirac Hamiltonians, i.e., $H' = \mathbf{h}' \cdot \boldsymbol{\gamma}$ and $H'' = \mathbf{h}'' \cdot \boldsymbol{\gamma}$. Therefore, the time evolution operator in general is given by $U(T; t_*) = u_c - i \sum_i u_i \gamma_i - \sum_{i < j} u_{ij} \gamma_i \gamma_j$ for certain coefficients u_c, u_i and u_{ij} . On the other hand, since $H_F^{(t_*)} = U^\dagger(0, -t_*) H_F U(0, -t_*)$, we have $[H_F^{(t_*)}]^2 = |\mathbf{h}_F|^2$ and $U(T; t_*) = \cos(|\mathbf{h}_F| T) - i \sin(|\mathbf{h}_F| T) H_F^{(t_*)} / |\mathbf{h}_F|$. Thus the Floquet Hamiltonian with reference time t_* takes the form of

$$H_F^{(t_*)}(\mathbf{k}) = \sum_{0 \leq i \leq d'} h_{F,i}^{(t_*)}(\mathbf{k}) \gamma_i + \sum_{0 \leq i < j \leq d'} h_{F,ij}^{(t_*)}(\mathbf{k}) i \gamma_i \gamma_j. \quad (11)$$

For this Hamiltonian, our dynamical characterization may not be directly applicable in general, since measuring the stroboscopic spin polarization $\langle \gamma_i(nT) \rangle = \text{Tr}[\rho_0 U^\dagger(nT; t_*) \gamma_i U(nT; t_*)]$ is equivalent to detecting the observable $U(0, -t_*) \gamma_i U^\dagger(0, -t_*)$ in the quantum quench dynamics governed by Floquet Hamiltonian H_F and with initial state $\rho_0^{(t_*)} = U(0, -t_*) \rho_0 U^\dagger(0, -t_*)$, which is quite complicated and from which the BISs are hard to be extracted.

Nevertheless, there exist a broad range of driving protocols with $h_i[\mathbf{k}; \boldsymbol{\lambda}(t)] = f(t)h_i(\mathbf{k}; \boldsymbol{\lambda})$ for all $i > 0$ and certain periodic function f , such as the models with hopping coefficients being driven by the same function, to which our dynamical characterization still can be applied directly. Here the quench process is still along the axis γ_0 . For these protocols, we have $H'(\mathbf{k}) = h'_0(\mathbf{k})\gamma_0 + \chi'(\mathbf{k})\sum_{i>0} h_i(\mathbf{k})\gamma_i$ and $H''(\mathbf{k}) = h''_0(\mathbf{k})\gamma_0 + \chi''(\mathbf{k})\sum_{i>0} h_i(\mathbf{k})\gamma_i$ by using the trick shown in Appendix C, and the corresponding Floquet Hamiltonian satisfies $h_{F,i}^{(t_*)}(\mathbf{k}) = \chi^{(t_*)}(\mathbf{k})h_i(\mathbf{k})$ and $h_{F,ij}^{(t_*)}(\mathbf{k}) = 0$ for $0 < i < j$, where χ 's are certain even functions. Although the Floquet Hamiltonian still takes a complicated form with nonzero $h_{F,0i}^{(t_*)}$, the corresponding stroboscopic time-averaged spin polarization now simplifies to $\overline{\langle \gamma_i(\mathbf{k}) \rangle} = -h_{F,0}^{(t_*)}h_{F,i}^{(t_*)}/|\mathbf{h}_F|^2$, which effectively measures the Z_2 topology of the Floquet Hamiltonian

$$\tilde{H}_F^{(t_*)}(\mathbf{k}) = h_{F,0}^{(t_*)}(\mathbf{k})\gamma_0 + \sum_{i>0} h_{F,i}^{(t_*)}(\mathbf{k})\gamma_i. \quad (12)$$

This Floquet phase may be gapless when both $h_{F,0}^{(t_*)}$ and $\chi^{(t_*)}$ vanish at certain momenta for certain t_* . However, we can prove that the effective Hamiltonian $\tilde{H}_F^{(t_*)}$ has the same Floquet Z_2 invariant as $H(\mathbf{k}, t)$ whenever it is gapped; see Appendix E. Therefore, the dynamical topological patterns emerging in the spin texture $\overline{\langle \gamma_i(\mathbf{k}) \rangle}$ still characterize the desired Z_2 Floquet topology. Note that the 1D Floquet topological phases of class D are very special, for which the Floquet Hamiltonian always takes the form of Dirac Hamiltonian and the above requirement for the periodic driving is not necessary.

As an example, we consider the 2D time-reversal invariant Floquet topological phase studied in Sec. III C but now with reference time $t_* = 0.45T$. It is clear that the above requirement for the driving protocol is satisfied. The directly measured stroboscopic time-averaged spin textures are shown in Figs. 4(a0)-4(a4). Compared with the results for $t_* = 0$ (cf. Fig. 3), the 1D 3-BISs⁽⁰⁾ with $h_{F,0} = 0$ in the π quasienergy gap and across the boundaries of Brillouin zone now disappear. As these BISs does not encircle any topological charge momentum with $h_{F,i} = 0$ for all $i > 0$, this change does not close the quasienergy gaps, and the Z_2 Floquet topology is unaffected. On the other hand, for the 3-BISs⁽⁰⁾ encircling the zero momentum, only the positions are slightly deformed. We note that $\tilde{H}_F^{(t_*)}$ is the exact Floquet Hamiltonian when $t_* = 0$ or $T/2$. When increasing t_* from zero

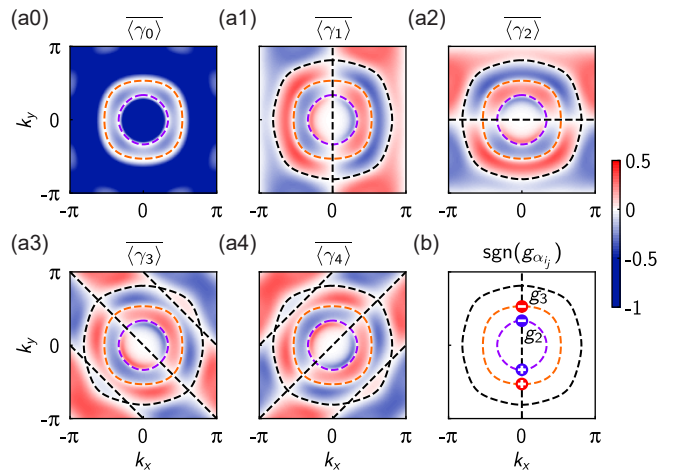


Figure 4. Direct measurement of the 2D time-reversal invariant Floquet topological phase with reference time $t_* = 0.45T$. (a0)-(a4) Stroboscopic time-averaged spin textures, from which the 1D 3-BISs⁽⁰⁾ with vanishing $h_{F,0}^{(t_*)}$ in the 0 quasienergy gap (orange dashed line) and π quasienergy gap (purple dashed line) as well as the 3-BISs⁽ⁱ⁾ with $h_{F,i}^{(t_*)} = 0$ for $i > 0$ (black dashed lines) can be identified. (b) The 0D 4-BISs (red and blue dots) constructed from 3-BISs⁽⁰⁾ and 3-BISs⁽¹⁾ and the corresponding dynamical field $g_{\alpha_{ij}}$. The resulting Floquet Z_2 invariants are given by $\nu_0 = -1$ and $\nu_\pi = -1$. The parameters are the same as in Fig. 3.

to $T/2$, the 3-BISs⁽⁰⁾ evolve from the one at $t_* = 0$ into those at $t_* = T/2$, during which the relative positions of BISs in the 0 and π gaps in general do not change.

The 3-BISs⁽ⁱ⁾ with vanishing $h_{F,i}^{(t_*)}$ for $i > 0$ can also be identified from the spin textures. Now the momenta with $\chi^{(t_*)} = 0$ (black dashed circles in Fig. 4) have moved from the region between 3-BISs⁽⁰⁾ and 3-BISs⁽⁰⁾ (cf. Fig. 3) to the outside region, manifesting that there exists reference time $0 < t'_* < t_*$ such that $h_{F,0}^{(t'_*)} = \chi^{(t'_*)} = 0$ for the considered model and the corresponding effective Hamiltonian $\tilde{H}_F^{(t'_*)}$ becomes gapless [note that $\tilde{H}_F^{(t_*)}$ is gapped]. The range for these t'_* is quite small from the numerical calculations, which does not affect most of the dynamical characterizations. Indeed, the dynamical topological pattern shown in Fig. 4(b) characterizes the desired Z_2 Floquet topology.

B. Modified stroboscopic time averages

For more general Floquet topological systems with reference time t_* , although the direct measurements are no longer applicable, our dynamical characterization scheme still works after slight modifications. First, instead of measuring from time $t = 0$, we consider the modified

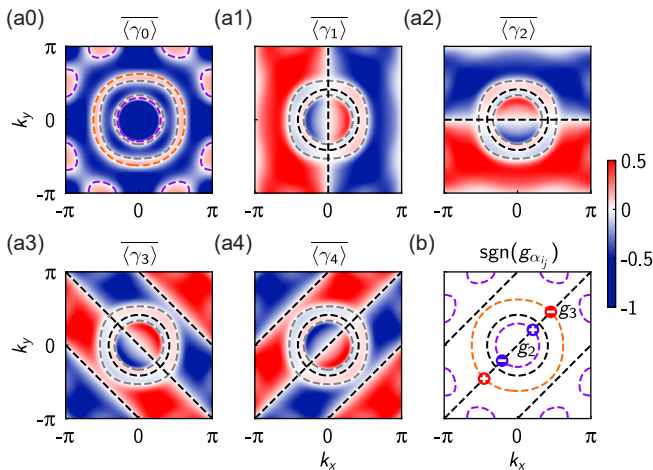


Figure 5. Characterizing the 2D time-reversal invariant Floquet topological phase with reference time $t_* = 0.45T$ via modified stroboscopic time averages. (a0-a4) The modified stroboscopic time-averaged spin textures. Here the gray dashed lines represent the dBISs, on which the spin polarizations $\overline{\langle \gamma_\alpha(\mathbf{k}; t_*) \rangle}$ vanish for all α . In each spin texture $\overline{\langle \gamma_i(\mathbf{k}; t_*) \rangle}$ for $i = 0, 1, \dots, 4$, other dashed lines (orange, purple, or black) represent the 3-BISs⁽ⁱ⁾ with $h_{F,i} = 0$. (b) Topological pattern. Here the highest-order 4-BISs (red or blue dots) are constructed from the 3-BISs⁽⁰⁾ in 0 (orange) or π (purple) quasienergy gaps and the 3-BISs⁽⁴⁾. The corresponding dynamical field g_3 and g_2 give us the Floquet Z_2 invariants $\nu_0 = -1$ and $\nu_\pi = -1$. The parameters are the same as in Fig. 3.

stroboscopic time-averaged spin polarizations [69]

$$\overline{\langle \gamma_i(\mathbf{k}; t_*) \rangle} \equiv \lim_{N \rightarrow \infty} \frac{1}{N} \sum_{n=0}^{N-1} \langle \gamma_i(\mathbf{k}, t = t_* + nT) \rangle. \quad (13)$$

Note that due to $U(t_* + nT; t_*) = U(nT, 0) \cdot U(0, -t_*)$, the spin polarization $\langle \gamma_i(t = t_* + nT) \rangle$ is equivalent to measuring the operator γ_i at $t = nT$ under the time evolution of Floquet Hamiltonian H_F with initial state $\rho_0^{(t_*)} = U(0, -t_*)\rho_0 U^\dagger(0, -t_*)$. Hence the time-averaged spin textures are given by

$$\overline{\langle \gamma_i(\mathbf{k}; t_*) \rangle} = h_{F,i}(\mathbf{k}) \text{Tr}[\rho_0^{(t_*)}(\mathbf{k}) H_F(\mathbf{k})] / |h_F(\mathbf{k})|^2. \quad (14)$$

This is similar to the shallow quench from an incompletely polarized initial state studied in Ref. [76].

The Z_2 Floquet topology can be identified by slightly modifying the definition of BISs and dynamical fields. One can see that each spin texture $\overline{\langle \gamma_i(\mathbf{k}; t_*) \rangle}$ vanishes on the momentum subspace given by either $\text{Tr}[\rho_0^{(t_*)}(\mathbf{k}) H_F(\mathbf{k})] = 0$ or $h_{F,i}(\mathbf{k}) = 0$. Here we define the former as the dynamical band-inversion surface (dBIS) with the following characteristic

$$\text{dBIS} = \{\mathbf{k} | \overline{\langle \gamma_\alpha(\mathbf{k}; t_*) \rangle} = 0, \forall \alpha\},$$

which is induced by the quantum quench dynamics for Floquet topological phases with nonzero t_* instead of the

Floquet Hamiltonian. Obviously, the dynamical band-inversion surface coincides with the $(d-1)$ D lowest-order $(d' - d + 1)$ -BIS⁽⁰⁾ with vanishing $h_{F,0}$ for the special case $t_* = 0$. However, they are different in general. The $(d' - d + 1)$ -BIS⁽ⁱ⁾ with $h_{F,i} = 0$ ($i = 0, 1, \dots, d'$) now is captured by the momenta with vanishing $\overline{\langle \gamma_i(\mathbf{k}; t_*) \rangle}$ while not on the dBIS. With these basic BISs, the higher-order n -BISs can be constructed in the same way as shown in Eq. (7). Further, since the spin polarization $\overline{\langle \gamma_i(\mathbf{k}; t_*) \rangle}$ does not always vanish on the highest-order BISs, the dynamical field can be modified as

$$g_i(\mathbf{k}) = \begin{cases} -(1/\mathcal{N}_{\mathbf{k}}) \partial_{k_\perp} \overline{\langle \gamma_i(\mathbf{k}; t_*) \rangle} & \text{if } \mathbf{k} \text{ is also on dBIS,} \\ \zeta_{\mathbf{k}} (1/\mathcal{N}_{\mathbf{k}}) \overline{\langle \gamma_i(\mathbf{k}; t_*) \rangle} & \text{otherwise,} \end{cases} \quad (15)$$

for $\mathbf{k} \in d'$ -BIS. Here k_\perp is perpendicular to the dBIS and points to the side with negative $\zeta_{\mathbf{k}} = \text{sgn}(\text{Tr}[\rho_0^{(t_*)} H_F])$. Given these modifications, the Z_2 Floquet invariant (8) remains unchanged.

In Figs. 5(a0)-5(a4), we show the modified stroboscopic time-averaged spin textures for the example of 2D time-reversal invariant Floquet topological phase with reference time $t_* = 0.45T$. Both the dBIS and 3-BISs⁽ⁱ⁾ with $h_{F,i} = 0$ for $i = 0, 1, \dots, 4$ can be identified. Recall that choosing which Floquet Hamiltonian coefficient to define the highest-order BISs is actually not unique. Here we choose the 3-BISs⁽⁰⁾ and 3-BISs⁽⁴⁾ to construct the highest-order 4-BISs [Fig. 5(b)], which have different positions compared with those shown in Fig. 3. Nevertheless, the dynamical Floquet Z_2 invariants ν_0 and ν_π remain unchanged, where the corresponding dynamical fields g_{α_i} now are chosen from the set $\{g_1, g_2, g_3\}$.

V. CONCLUSION

In conclusion, we have established the first full and unified dynamical characterization theory for Z_2 Floquet topological phases of different dimensionality and tenfold-way symmetry classes using the minimal information about the Floquet bands. We show that the Floquet Z_2 topology can be completely characterized by the topological patterns emerging in the quantum dynamics induced by quenching the system from a trivial and static initial state to the Floquet topological regime. Particularly, the dynamical Z_2 invariants defined on the 0D highest-order BISs in the 0 and π quasienergy gaps uniquely capture the corresponding Floquet boundary modes, hence providing a full dynamical characterization for the Z_2 Floquet topological phases both in the conventional and anomalous sense.

Our theory can be applied to a broad range of periodically driven systems, and the measured quantities are easily accessible in current experiments. Therefore, our work shall advance the experimental studies of Z_2 Floquet topological phases. Especially, for the quantum simulation platforms based on ultracold atoms or solid-

state spin systems, where the boundary physics is hard to simulate and measure, our dynamical characterization scheme based on the BISs is extremely useful and provides a highly feasible method to detect the bulk topology. On the other hand, our work completes the dynamical characterization for the full tenfold classes of Floquet topological phases, which shall advance this research topic. Especially, it would be interesting to further generalize our theory into more broad Floquet topological systems, such as those protected by the crystalline or space-time symmetries [102–104], which is a meaningful future direction.

ACKNOWLEDGMENTS

We acknowledge support from: ERC AdG NO-QIA; MCIN/AEI (PGC2018-0910.13039/501100011033, CEX2019-000910-S/10.13039/501100011033, Plan National FIDEUA PID2019-106901GB-I00, Plan National STAMEENA PID2022-139099NB-I00 project funded by MCIN/AEI/10.13039/501100011033 and by the “European Union NextGenerationEU/PRTR” (PRTR-C17.I1), FPI); QUANTERA MAQS PCI2019-111828-2); QUANTERA DYNAMITE PCI2022-132919 (QuantERA II Programme co-funded by European Union’s Horizon 2020 program under Grant Agreement No 101017733), Ministry of Economic Affairs and Digital Transformation of the Spanish Government through the QUANTUM ENIA project call – Quantum Spain project, and by the European Union through the Recovery, Transformation, and Resilience Plan – NextGenerationEU within the framework of the Digital Spain 2026 Agenda; Fundació Cellex; Fundació Mir-Puig; Generalitat de Catalunya (European Social Fund FEDER and CERCA program, AGAUR Grant No. 2021 SGR 01452, QuantumCAT \ U16-011424, co-funded by ERDF Operational Program of Catalonia 2014-2020); Barcelona Supercomputing Center MareNostrum (FI-2023-1-0013); EU Quantum Flagship (PASQuanS2.1, 101113690); EU Horizon 2020 FET-OPEN OPTologic (Grant No 899794); EU Horizon Europe Program (Grant Agreement 101080086 – NeQST), ICFO Internal “QuantumGaudi” project; European Union’s Horizon 2020 program under the Marie-Sklodowska-Curie grant agreement No 847648; “La Caixa” Junior Leaders fellowships, “La Caixa” Foundation (ID 100010434): CF/BQ/PR23/11980043. Views and opinions expressed are, however, those of the author(s) only and do not necessarily reflect those of the European Union, European Commission, European Climate, Infrastructure and Environment Executive Agency (CINEA), or any other granting authority. Neither the European Union nor any granting authority can be held responsible for them.

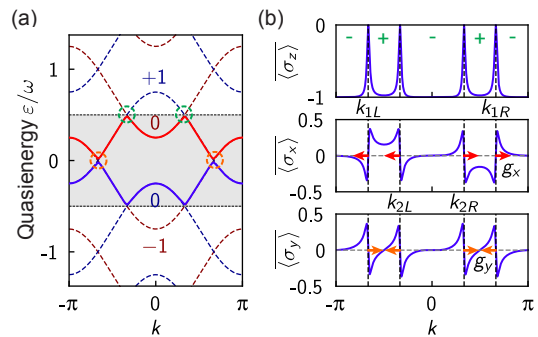


Figure 6. Dynamical characterization of the 1D Floquet topological phase (1) with weak spin-orbit coupling but strong periodic driving. (a) Quasienergy band structure. The solid lines represent the Floquet bands, while the red and blue dashed lines are the copied and shifted decoupled h_z -bands labeled by $m = 0, \pm 1, \dots$ and with $\sigma_z = \pm 1$, respectively. The orange (green) dashed circles highlight the BISs in the 0 (π) quasienergy gap. (b) Stroboscopic time-averaged spin textures. The vanishing spin polarizations in all directions determine the 2-BIS₀ points $k_{1L(R)}$ and the 2-BIS _{π} points $k_{2L(R)}$. The corresponding nonzero dynamical fields $g_{x,y}$ are shown in red (or orange) arrows. In $\langle \overline{\sigma_z} \rangle$, we also label the regions with $h_{F,z} \geq 0$ using the symbols “ \pm ”, respectively. Here we set $\mu_0 = 3t_0$, $\mu_d = 25t_0$, $\Delta = 0.2t_0$, and $\omega = 4t_0$.

Appendix A: Strong periodic driving or spin-orbit coupling

In this Appendix, we provide examples to show that our dynamical characterization theory of Z_2 Floquet topological phases based on the BISs can be applied to the cases with weak (strong) spin-orbit coupling but strong (weak) periodic driving.

1. Weak spin-orbit coupling but strong periodic driving

We first consider the cases with weak spin-orbit coupling but strong periodic driving. As an example, in Fig. 6 we show numerical results for the 1D Floquet topological phase (1) with spin-orbit coupling $\Delta = 0.2t_0$ and periodic driving strength $\mu_d = 25t_0$. By comparing the band crossings in the Floquet band structure [Fig. 6(a)] and the BISs observed in the stroboscopic time-averaged spin polarizations [Fig. 6(b)], we can conclude that the 0 and π gap BISs still can be determined by the decoupled h_z -bands for the cases with weak spin-orbit coupling but strong periodic driving. Moreover, the opposite dynamical fields $g_{x,y}$ on the 2-BIS_{0, π} manifest the nontrivial Z_2 Floquet invariant $\nu_0 = \nu_\pi = -1$, consistent with the edge modes in each quasienergy gap as we numerically checked. This demonstrates the validity of our dynamical characterization theory in this case.

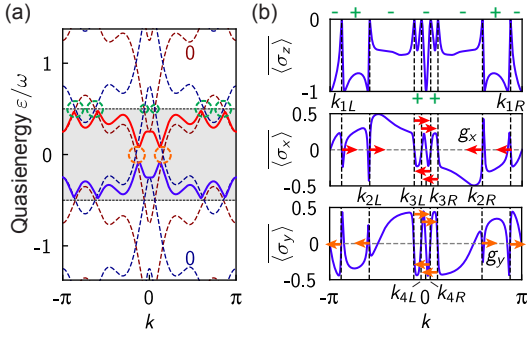


Figure 7. Dynamical detection of the 1D Floquet topological phase (1) with strong spin-orbit coupling but weak periodic driving. (a) Quasienergy band structure. The solid lines represent the Floquet bands, while the red (blue) dashed lines are the copied and shifted upper (lower) static bands with spin-orbit coupling taken into account. Here the orange and green dashed circles highlight the band crossings in the 0 and π quasienergy gaps, respectively. (b) Stroboscopic time-averaged spin textures. The vanishing spin polarizations in all directions identify the 2-BIS₀ points $k_{3L(R)}$ and the 2-BIS _{π} points $k_{1,2,4L(R)}$. The corresponding dynamical fields $g_{x,y}$ are shown in red (orange) arrows. We also label the regions with $h_{F,z} \geq 0$ in $\langle \sigma_z \rangle$ using the symbols “ \pm ”, respectively. Here we set $\mu_0 = 3t_0$, $\mu_d = 3t_0$, $\Delta = 2t_0$, and $\omega = 4t_0$.

2. Strong spin-orbit coupling but weak periodic driving

We now study the cases with strong spin-orbit coupling but weak periodic driving by considering the 1D Floquet topological phase (1) with $\Delta = 2t_0$ and $\mu_d = 3t_0$. The numerical results are shown in Fig. 7. Clearly, the BISs observed in the quantum quench dynamics [Fig. 7(b)] cannot be identified from the decoupled h_z bands but are determined by the copied and shifted static bands with spin-orbit coupling taken into account [see Fig. 7(a)], as the spin-orbit coupling strongly deforms the decoupled bands and induces additional π gap BIS momentum points $k_{1,2L(R)}$. Since there is no band crossings in the static Hamiltonian for our parameters, using the copied and shifted static bands is enough to determine all the BISs. Otherwise, we have to use the decoupled bands to identify the 0 gap BISs for the static Hamiltonian, which are opened by the spin-orbit coupling when considering the static bands. Using the general Z_2 Floquet invariant (8), we have $\nu_0 = \nu_\pi = -1$ according to the dynamical fields $g_{x,y}$ on the BISs [see Fig. 7(b)]. We checked that this is consistent with the edge modes in each quasienergy gap. Hence our dynamical characterization theory is also valid for the cases with strong spin-orbit coupling but weak periodic driving.

Appendix B: Symmetry constraints on the periodic driving

In this Appendix, we discuss the symmetry constraints imposed on the periodically driven parameters $\lambda_\ell(t)$. Here we denote $h_{o(e)}(\mathbf{k}; \boldsymbol{\lambda})$ to be one of the static Hamiltonian coefficient of parity odd (even) with respect to the momentum \mathbf{k} .

We consider the time-reversal symmetry Θ , the particle-hole symmetry Ξ , and the chiral symmetry Π , satisfying

$$\begin{aligned} \Theta H(\mathbf{k}, t) \Theta^{-1} &= H(-\mathbf{k}, -t), \\ \Xi H(\mathbf{k}, t) \Xi^{-1} &= -H(-\mathbf{k}, t), \\ \Pi H(\mathbf{k}, t) \Pi^{-1} &= -H(\mathbf{k}, -t). \end{aligned} \quad (\text{B1})$$

Here Θ and Ξ are anti-unitary operators, while Π is a unitary operator. Under these symmetries, the matrix γ_i transforms as

$$\begin{aligned} \Theta: \quad \gamma_o &\rightarrow -\gamma_o, \quad \gamma_e \rightarrow \gamma_e, \\ \Xi: \quad \gamma_o &\rightarrow \gamma_o, \quad \gamma_e \rightarrow -\gamma_e, \\ \Pi: \quad \gamma_o &\rightarrow -\gamma_o, \quad \gamma_e \rightarrow -\gamma_e, \end{aligned} \quad (\text{B2})$$

which can be identified from the static Hamiltonian. Therefore, in the Floquet regime we have

$$\begin{aligned} h_o[\mathbf{k}; \boldsymbol{\lambda}(t)] &= -h_o[-\mathbf{k}; \boldsymbol{\lambda}(-t)] = h_o[\mathbf{k}; \boldsymbol{\lambda}(-t)], \\ h_e[\mathbf{k}; \boldsymbol{\lambda}(t)] &= h_e[-\mathbf{k}; \boldsymbol{\lambda}(-t)] = h_e[\mathbf{k}; \boldsymbol{\lambda}(-t)] \end{aligned} \quad (\text{B3})$$

for the time-reversal symmetry, and

$$h_{o(e)}[\mathbf{k}; \boldsymbol{\lambda}(t)] = h_{o(e)}[\mathbf{k}; \boldsymbol{\lambda}(-t)] \quad (\text{B4})$$

for the chiral symmetry, leading to the result

$$\boldsymbol{\lambda}(t) = \boldsymbol{\lambda}(-t). \quad (\text{B5})$$

On the other hand, the particle-hole symmetry only requires $h_o[\mathbf{k}; \boldsymbol{\lambda}(t)] = -h_o[-\mathbf{k}; \boldsymbol{\lambda}(t)]$ and $h_e[\mathbf{k}; \boldsymbol{\lambda}(t)] = h_e[-\mathbf{k}; \boldsymbol{\lambda}(t)]$, which does not impose any constraint on the periodic driving $\boldsymbol{\lambda}(t)$. Nevertheless, we also assume the above requirement for Floquet topological phases only with the particle-hole symmetry and of dimensionality $d > 3$ in this work, which has covered a broad range of topological states.

Appendix C: Floquet Hamiltonian H_F

In this Appendix, we show that the Floquet Hamiltonian for the periodically driven model (5) can be written as $H_F = \mathbf{h}_F \cdot \boldsymbol{\gamma}$. The proof is straightforward. We note that the Floquet Hamiltonian is given by $H_F = (i/T) \log U(T)$ with

$$\begin{aligned} U(t) &= e^{-iH(T)\delta T} \{ \dots [e^{-iH(T/2+2\delta t)\delta t} (e^{-iH(T/2+\delta t)\delta t} \\ &\quad \times e^{-iH(T/2)\delta t} e^{-iH(T/2-\delta t)\delta t}) e^{-iH(T-2\delta t)\delta t}] \dots \} \\ &\quad \times e^{-iH(0)\delta t}, \end{aligned} \quad (\text{C1})$$

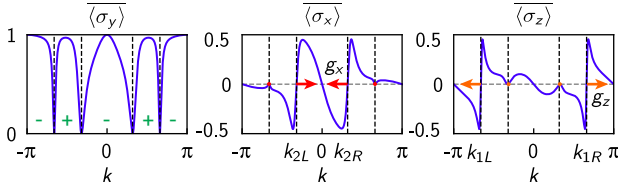


Figure 8. Stroboscopic time-averaged spin textures for the rotated Hamiltonian (D1). The vanishing spin polarizations in all directions determine the 2-BIS₀ points $k_{1L(R)}$ and the 2-BIS _{π} points $k_{2L(R)}$; cf. Fig. 1(a). The corresponding dynamical fields $g_{x,z}$ are shown in red (or orange) arrows, while the dots indicate that the dynamical field vanishes on these momentum points. In $\langle \sigma_y \rangle$, we also label the regions with $h_{F,y} \geq 0$ using the symbols “+”, respectively. Here the parameters are the same as in Fig. 1(d).

where $\delta\tau$ is an infinitesimal time interval and $\exp(-iH\delta\tau) = \cos(|\mathbf{h}|\delta\tau) - i \sin(|\mathbf{h}|\delta\tau)H/|\mathbf{h}|$. After some algebra, one can readily show that

$$\begin{aligned} & e^{-iH(T/2+\delta t)\delta t} e^{-iH(T/2)\delta t} e^{-iH(T/2-\delta t)\delta t} \\ & = u_c - i \sum_i u_i \gamma_i \equiv e^{-i(\tilde{\mathbf{h}} \cdot \boldsymbol{\gamma}) \cdot 3\delta t} \end{aligned} \quad (\text{C2})$$

for the 1D Floquet topological phases of class D or for the symmetry constrained periodic driving $h_i(\mathbf{k}, t) = h_i(\mathbf{k}, -t)$, where u_c and u_i are certain functions of the Hamiltonian coefficients $h_i(T/2)$ and $h_i(T/2 \pm \delta\tau)$. Repeating this procedure, i.e., calculating $\exp[-iH(T/2 + 2\delta\tau)\delta\tau] \exp[-i(\tilde{\mathbf{h}} \cdot \boldsymbol{\gamma}) \cdot 3\delta\tau] \exp[-iH(T/2 - 2\delta\tau)\delta\tau]$ and so on, we can obtain $H_F = \mathbf{h}_F \cdot \boldsymbol{\gamma}$.

Appendix D: Basis change of Hamiltonians

Here we show that our dynamical characterization is not affected by the basis change of Hamiltonians, if the resulting Hamiltonian coefficients are still either odd or even with respect to the momentum \mathbf{k} . As an example, we consider the Hamiltonian (1) rotated about the σ_x axis by 90° followed by a rotation about the σ_y axis by 45° . The corresponding Hamiltonian is given by

$$\begin{aligned} H(k, t) &= \sqrt{2}\Delta(\sin k + \sin 2k)\sigma_x - [\mu(t) - 2t_0 \cos k]\sigma_y \\ &\quad - \sqrt{2}\Delta(\sin k - \sin 2k)\sigma_z. \end{aligned} \quad (\text{D1})$$

Compared with Eq. (1), the Hamiltonian coefficients are rotated among each other but still satisfy the even or odd properties. Similar to Fig. 1, we consider the quantum dynamics induced by quenching the fully polarized initial state with $\mu_0 \gg t_0, \omega$ (now along the σ_y axis) to the Floquet topological regime with $\mu_0 = 3t_0$, $\mu_d = 3t_0$, $\Delta = 0.2t_0$, and $\omega = 4t_0$. The results are presented in Fig. 8. Although the spin textures are totally different

from those shown in Fig. 1(d), the BISs still can be identified from the momentum points with vanishing spin polarizations in all directions. Moreover, although g_x and g_z may vanish on certain BIS points, the nonzero and opposite dynamical fields g_z (g_x) on the 2-BIS₀ points $k_{1L(R)}$ [2-BIS _{π} points $k_{2L(R)}$] still characterize correctly the nontrivial Z_2 topology in the 0 (π) quasienergy gap, respectively; cf. Fig. 1(b). Hence our dynamical characterization theory is not affected by the basis change of Hamiltonians.

Appendix E: Effective Hamiltonian $\tilde{H}_F^{(t_*)}$ for direct measurements

In this Appendix, we study the quasienergy gap of the Floquet phase associated with $\tilde{H}_F^{(t_*)}(\mathbf{k}) = h_{F,0}^{(t_*)}(\mathbf{k})\gamma_0 + \sum_{i>0} h_{F,i}^{(t_*)}(\mathbf{k})\gamma_i$ and its topological properties, where we have $h_{F,i}^{(t_*)}(\mathbf{k}) = \chi^{(t_*)}(\mathbf{k})h_i(\mathbf{k})$ for $i > 0$ with $\chi^{(t_*)}(\mathbf{k})$ being certain even function [cf. Eq. (12)]. In the following, we denote $\tilde{\mathbf{h}}_F^{(t_*)} \equiv (h_{F,0}^{(t_*)}, h_{F,1}^{(t_*)}, \dots, h_{F,d'}^{(t_*)})$ for brevity.

We note that the Floquet Hamiltonian for reference time t_* is given by $H_F^{(t_*)}(\mathbf{k}) = \sum_{0 \leq i \leq d'} h_{F,i}^{(t_*)}(\mathbf{k})\gamma_i + \sum_{i>0} h_{F,0i}^{(t_*)}(\mathbf{k})i\gamma_0\gamma_i$. Since $|\tilde{\mathbf{h}}_F^{(t_*)}|$ is smaller than the quasienergy of Floquet Hamiltonian, $(|\tilde{\mathbf{h}}_F^{(t_*)}|^2 + \sum_{0 < i \leq d'} [h_{F,0i}^{(t_*)}]^2)^{1/2} < \pi/T$, the Floquet phase associated with $\tilde{H}_F^{(t_*)}$ is indeed gapped in the π quasienergy gap. On the other hand, for the 0 quasienergy gap, we notice that $h_{F,0}^{(t_*)}$ equals $h_{F,0}$ and is nonzero at the momenta where $h_i = 0$ for all $i > 0$. Thus $\tilde{\mathbf{h}}_F^{(t_*)}$ is always finite whenever $\chi^{(t_*)} \neq 0$. The effective Hamiltonian $\tilde{H}_F^{(t_*)}$ can be gapless only when both $h_{F,0}^{(t_*)}$ and $\chi^{(t_*)}$ vanish at certain momenta for certain t_* . In general, the range of these t_* is quite small, and $\tilde{H}_F^{(t_*)}$ is fully gapped for most cases.

To study the topological properties, we consider a family of Hamiltonians $\tilde{H}_F^{(t_*)}$ parameterized by t_* . For $t_* = 0$, the effective Hamiltonian gives the exact Floquet Hamiltonian H_F . Clearly, $\tilde{H}_F^{(t_*)}$ and H_F possess the same symmetries. If the 0 and π quasienergy gaps are always gapped for all t_* , then the Floquet phase associated with $\tilde{H}_F^{(t_*)}$ has the same Z_2 topology as the original phase $H(\mathbf{k}, t)$. This is also valid for the cases whenever $\tilde{H}_F^{(t_*)}$ is gapped, although there may be certain reference time between 0 and t_* at which the effective Hamiltonian becomes gapless. The point is that since both $h_{F,0}^{(t_*)}$ and $\chi^{(t_*)}$ are even functions of \mathbf{k} , the close and reopening of 0 quasienergy gap for each Floquet band must occur at pairs of symmetric momentum points, which shall not affect the Z_2 topology [105]. This completes the proof.

- [1] R. B. Laughlin, Quantized Hall conductivity in two dimensions, *Phys. Rev. B* **23**, 5632 (1981).
- [2] D. C. Tsui, H. L. Stormer, and A. C. Gossard, Two-Dimensional Magnetotransport in the Extreme Quantum Limit, *Phys. Rev. Lett.* **48**, 1559 (1982).
- [3] R. B. Laughlin, Anomalous Quantum Hall Effect: An Incompressible Quantum Fluid with Fractionally Charged Excitations, *Phys. Rev. Lett.* **50**, 1395 (1983).
- [4] K. v. Klitzing, G. Dorda, and M. Pepper, New Method for High-Accuracy Determination of the Fine-Structure Constant Based on Quantized Hall Resistance, *Phys. Rev. Lett.* **45**, 494 (1980).
- [5] D. J. Thouless, M. Kohmoto, M. P. Nightingale, and M. den Nijs, Quantized Hall Conductance in a Two-Dimensional Periodic Potential, *Phys. Rev. Lett.* **49**, 405 (1982).
- [6] L. D. Landau and E. M. Lifshitz, *Statistical Physics* (Elsevier, 2013).
- [7] C. L. Kane and E. J. Mele, Quantum Spin Hall Effect in Graphene, *Phys. Rev. Lett.* **95**, 226801 (2005).
- [8] C. L. Kane and E. J. Mele, Z_2 Topological Order and the Quantum Spin Hall Effect, *Phys. Rev. Lett.* **95**, 146802 (2005).
- [9] B. A. Bernevig and S.-C. Zhang, Quantum Spin Hall Effect, *Phys. Rev. Lett.* **96**, 106802 (2006).
- [10] M. König, S. Wiedmann, C. Brüne, A. Roth, H. Buhmann, L. W. Molenkamp, X.-L. Qi, and S.-C. Zhang, Quantum Spin Hall Insulator State in HgTe Quantum Wells, *Science* **318**, 766 (2007).
- [11] A. Altland and M. R. Zirnbauer, Nonstandard symmetry classes in mesoscopic normal-superconducting hybrid structures, *Phys. Rev. B* **55**, 1142 (1997).
- [12] A. P. Schnyder, S. Ryu, A. Furusaki, and A. W. W. Ludwig, Classification of topological insulators and superconductors in three spatial dimensions, *Phys. Rev. B* **78**, 195125 (2008).
- [13] A. Kitaev, Periodic table for topological insulators and superconductors, *AIP Conf. Proc.* **1134**, 22 (2009).
- [14] S. Ryu, A. P. Schnyder, A. Furusaki, and A. W. W. Ludwig, Topological insulators and superconductors: tenfold way and dimensional hierarchy, *New J. Phys.* **12**, 065010 (2010).
- [15] M. Z. Hasan and C. L. Kane, Colloquium: Topological insulators, *Rev. Mod. Phys.* **82**, 3045 (2010).
- [16] X.-L. Qi and S.-C. Zhang, Topological insulators and superconductors, *Rev. Mod. Phys.* **83**, 1057 (2011).
- [17] C.-K. Chiu, J. C. Y. Teo, A. P. Schnyder, and S. Ryu, Classification of topological quantum matter with symmetries, *Rev. Mod. Phys.* **88**, 035005 (2016).
- [18] C.-Z. Chang, J. Zhang, X. Feng, J. Shen, Z. Zhang, M. Guo, K. Li, Y. Ou, P. Wei, L.-L. Wang, Z.-Q. Ji, Y. Feng, S. Ji, X. Chen, J. Jia, X. Dai, Z. Fang, S.-C. Zhang, K. He, Y. Wang, L. Lu, X.-C. Ma, and Q.-K. Xue, Experimental Observation of the Quantum Anomalous Hall Effect in a Magnetic Topological Insulator, *Science* **340**, 167 (2013).
- [19] Q. L. He, L. Pan, A. L. Stern, E. C. Burks, X. Che, G. Yin, J. Wang, B. Lian, Q. Zhou, E. S. Choi, K. Murata, X. Kou, Z. Chen, T. Nie, Q. Shao, Y. Fan, S.-C. Zhang, K. Liu, J. Xia, and K. L. Wang, Chiral Majorana fermion modes in a quantum anomalous Hall insulator-superconductor structure, *Science* **357**, 294 (2017).
- [20] D. Hsieh, D. Qian, L. Wray, Y. Xia, Y. S. Hor, R. J. Cava, and M. Z. Hasan, A topological Dirac insulator in a quantum spin Hall phase, *Nature* **452**, 970 (2008).
- [21] Y. L. Chen, J. G. Analytis, J.-H. Chu, Z. K. Liu, S.-K. Mo, X. L. Qi, H. J. Zhang, D. H. Lu, X. Dai, Z. Fang, S. C. Zhang, I. R. Fisher, Z. Hussain, and Z.-X. Shen, Experimental Realization of a Three-Dimensional Topological Insulator, Bi_2Te_3 , *Science* **325**, 178 (2009).
- [22] Y. Xia, D. Qian, D. Hsieh, L. Wray, A. Pal, H. Lin, A. Bansil, D. Grauer, Y. S. Hor, R. J. Cava, and M. Z. Hasan, Observation of a large-gap topological-insulator class with a single Dirac cone on the surface, *Nat. Phys.* **5**, 398 (2009).
- [23] T. Oka and H. Aoki, Photovoltaic Hall effect in graphene, *Phys. Rev. B* **79**, 081406 (2009).
- [24] T. Kitagawa, M. S. Rudner, E. Berg, and E. Demler, Exploring topological phases with quantum walks, *Phys. Rev. A* **82**, 033429 (2010).
- [25] T. Kitagawa, E. Berg, M. Rudner, and E. Demler, Topological characterization of periodically driven quantum systems, *Phys. Rev. B* **82**, 235114 (2010).
- [26] J. ichi Inoue and A. Tanaka, Photoinduced Transition between Conventional and Topological Insulators in Two-Dimensional Electronic Systems, *Phys. Rev. Lett.* **105**, 017401 (2010).
- [27] L. Jiang, T. Kitagawa, J. Alicea, A. R. Akhmerov, D. Pekker, G. Refael, J. I. Cirac, E. Demler, M. D. Lukin, and P. Zoller, Majorana Fermions in Equilibrium and in Driven Cold-Atom Quantum Wires, *Phys. Rev. Lett.* **106**, 220402 (2011).
- [28] N. H. Lindner, G. Refael, and V. Galitski, Floquet topological insulator in semiconductor quantum wells, *Nat. Phys.* **7**, 490 (2011).
- [29] T. Kitagawa, T. Oka, A. Brataas, L. Fu, and E. Demler, Transport properties of nonequilibrium systems under the application of light: Photoinduced quantum Hall insulators without Landau levels, *Phys. Rev. B* **84**, 235108 (2011).
- [30] Y. H. Wang, H. Steinberg, P. Jarillo-Herrero, and N. Gedik, Observation of Floquet-Bloch States on the Surface of a Topological Insulator, *Science* **342**, 453 (2013).
- [31] F. Mahmood, C.-K. Chan, Z. Alpichshev, D. Gardner, Y. Lee, P. A. Lee, and N. Gedik, Selective scattering between Floquet-Bloch and Volkov states in a topological insulator, *Nat. Phys.* **12**, 306 (2016).
- [32] G. Jotzu, M. Messer, R. Desbuquois, M. Lebrat, T. Uehlinger, D. Greif, and T. Esslinger, Experimental realization of the topological Haldane model with ultracold fermions, *Nature* **515**, 237 (2014).
- [33] N. Fläschner, B. S. Rem, M. Tarnowski, D. Vogel, D.-S. Lühmann, K. Sengstock, and C. Weitenberg, Experimental reconstruction of the Berry curvature in a Floquet Bloch band, *Science* **352**, 1091 (2016).
- [34] K. Wintersperger, C. Braun, F. N. Ünal, A. Eckardt, M. D. Liberto, N. Goldman, I. Bloch, and M. Aidelsburger, Realization of an anomalous Floquet topological system with ultracold atoms, *Nat. Phys.* **16**, 1058 (2020).
- [35] R.-J. Slager, A. Bouhon, and F. N. Ünal, Floquet multi-

- gap topology: Non-Abelian braiding and anomalous Dirac string phase, arXiv:2208.12824.
- [36] J. Cayssol, B. Dóra, F. Simon, and R. Moessner, Floquet topological insulators, *Phys. Status Solidi RRL* **7**, 101 (2013).
- [37] T. Nag, R.-J. Slager, T. Higuchi, and T. Oka, Dynamical synchronization transition in interacting electron systems, *Phys. Rev. B* **100**, 134301 (2019).
- [38] F. Harper, R. Roy, M. S. Rudner, and S. L. Sondhi, Topology and Broken Symmetry in Floquet Systems, *Annu. Rev. Condens. Matter Phys.* **11**, 345 (2020).
- [39] M. S. Rudner and N. H. Lindner, Band structure engineering and non-equilibrium dynamics in Floquet topological insulators, *Nat. Rev. Phys.* **2**, 229 (2020).
- [40] M. Jangjan and M. V. Hosseini, Floquet engineering of topological metal states and hybridization of edge states with bulk states in dimerized two-leg ladders, *Sci. Rep.* **10**, 14256 (2020).
- [41] P. Molignini, W. Chen, and R. Chitra, Universal quantum criticality in static and floquet-majorana chains, *Phys. Rev. B* **98**, 125129 (2018).
- [42] P. Molignini, W. Chen, and R. Chitra, Generating quantum multicriticality in topological insulators by periodic driving, *Phys. Rev. B* **101**, 165106 (2020).
- [43] P. Molignini, Edge mode manipulation through commensurate multifrequency driving, *Phys. Rev. B* **102**, 235143 (2020).
- [44] P. Molignini, A. G. Celades, R. Chitra, and W. Chen, Crossdimensional universality classes in static and periodically driven kitaev models, *Phys. Rev. B* **103**, 184507 (2021).
- [45] T. Nag and B. Roy, Anomalous and normal dislocation modes in Floquet topological insulators, *Commun. Phys.* **4**, 157 (2021).
- [46] A. K. Ghosh, T. Nag, and A. Saha, Systematic generation of the cascade of anomalous dynamical first- and higher-order modes in Floquet topological insulators, *Phys. Rev. B* **105**, 115418 (2022).
- [47] M. Jangjan, L. E. F. Foa Torres, and M. V. Hosseini, Floquet topological phase transitions in a periodically quenched dimer, *Phys. Rev. B* **106**, 224306 (2022).
- [48] M. Bukov, L. D'Alessio, and A. Polkovnikov, Universal high-frequency behavior of periodically driven systems: from dynamical stabilization to Floquet engineering, *Adv. Phys.* **64**, 139 (2015).
- [49] A. Eckardt, Colloquium: Atomic quantum gases in periodically driven optical lattices, *Rev. Mod. Phys.* **89**, 011004 (2017).
- [50] T. Kitagawa, M. A. Broome, A. Fedrizzi, M. S. Rudner, E. Berg, I. Kassal, A. Aspuru-Guzik, E. Demler, and A. G. White, Observation of topologically protected bound states in photonic quantum walks, *Nat. Commun.* **3**, 882 (2012).
- [51] M. S. Rudner, N. H. Lindner, E. Berg, and M. Levin, Anomalous Edge States and the Bulk-Edge Correspondence for Periodically Driven Two-Dimensional Systems, *Phys. Rev. X* **3**, 031005 (2013).
- [52] S. Yao, Z. Yan, and Z. Wang, Topological invariants of Floquet systems: General formulation, special properties, and Floquet topological defects, *Phys. Rev. B* **96**, 195303 (2017).
- [53] P. Xu, W. Zheng, and H. Zhai, Topological micromotion of Floquet quantum systems, *Phys. Rev. B* **105**, 045139 (2022).
- [54] F. Nathan and M. S. Rudner, Topological singularities and the general classification of Floquet-Bloch systems, *New J. Phys.* **17**, 125014 (2015).
- [55] R. Roy and F. Harper, Periodic table for Floquet topological insulators, *Phys. Rev. B* **96**, 155118 (2017).
- [56] C. Wang, P. Zhang, X. Chen, J. Yu, and H. Zhai, Scheme to Measure the Topological Number of a Chern Insulator from Quench Dynamics, *Phys. Rev. Lett.* **118**, 185701 (2017).
- [57] M. Tarnowski, F. N. Ünal, N. Fläschner, B. S. Rem, A. Eckardt, K. Sengstock, and C. Weitenberg, Measuring topology from dynamics by obtaining the Chern number from a linking number, *Nat. Commun.* **10**, 1728 (2019).
- [58] F. N. Ünal, A. Bouhon, and R.-J. Slager, Topological Euler Class as a Dynamical Observable in Optical Lattices, *Phys. Rev. Lett.* **125**, 053601 (2020).
- [59] T. Mizoguchi, Y. Kuno, and Y. Hatsugai, Detecting Bulk Topology of Quadrupolar Phase from Quench Dynamics, *Phys. Rev. Lett.* **126**, 016802 (2021).
- [60] J. C. Budich and M. Heyl, Dynamical topological order parameters far from equilibrium, *Phys. Rev. B* **93**, 085416 (2016).
- [61] C. Yang, L. Li, and S. Chen, Dynamical topological invariant after a quantum quench, *Phys. Rev. B* **97**, 060304 (2018).
- [62] Z. Gong and M. Ueda, Topological Entanglement-Spectrum Crossing in Quench Dynamics, *Phys. Rev. Lett.* **121**, 250601 (2018).
- [63] M. McGinley and N. R. Cooper, Topology of One-Dimensional Quantum Systems Out of Equilibrium, *Phys. Rev. Lett.* **121**, 090401 (2018).
- [64] X. Qiu, T.-S. Deng, Y. Hu, P. Xue, and W. Yi, Fixed Points and Dynamic Topological Phenomena in a Parity-Time-Symmetric Quantum Quench, *iScience* **20**, 392 (2019).
- [65] K. Wang, X. Qiu, L. Xiao, X. Zhan, Z. Bian, W. Yi, and P. Xue, Simulating Dynamic Quantum Phase Transitions in Photonic Quantum Walks, *Phys. Rev. Lett.* **122**, 020501 (2019).
- [66] M. McGinley and N. R. Cooper, Classification of topological insulators and superconductors out of equilibrium, *Phys. Rev. B* **99**, 075148 (2019).
- [67] H. Hu and E. Zhao, Topological Invariants for Quantum Quench Dynamics from Unitary Evolution, *Phys. Rev. Lett.* **124**, 160402 (2020).
- [68] K. Sim, R. Chitra, and P. Molignini, Quench dynamics and scaling laws in topological nodal loop semimetals, *Phys. Rev. B* **106**, 224302 (2022).
- [69] L. Zhang, L. Zhang, and X.-J. Liu, Unified Theory to Characterize Floquet Topological Phases by Quench Dynamics, *Phys. Rev. Lett.* **125**, 183001 (2020).
- [70] L. Zhang and X.-J. Liu, Unconventional Floquet Topological Phases from Quantum Engineering of Band-Inversion Surfaces, *PRX Quantum* **3**, 040312 (2022).
- [71] B.-B. Wang and L. Zhang, Characterizing Floquet topological phases by quench dynamics: A multiple-subsystem approach, arXiv:2310.08409.
- [72] L. Zhang, L. Zhang, S. Niu, and X.-J. Liu, Dynamical classification of topological quantum phases, *Sci. Bull.* **63**, 1385 (2018).
- [73] L. Zhang, L. Zhang, and X.-J. Liu, Dynamical detection of topological charges, *Phys. Rev. A* **99**, 053606 (2019).
- [74] L. Zhang, L. Zhang, and X.-J. Liu, Characterizing topo-

- logical phases by quantum quenches: A general theory, *Phys. Rev. A* **100**, 063624 (2019).
- [75] X.-L. Yu, W. Ji, L. Zhang, Y. Wang, J. Wu, and X.-J. Liu, Quantum Dynamical Characterization and Simulation of Topological Phases With High-Order Band Inversion Surfaces, *PRX Quantum* **2**, 020320 (2021).
- [76] L. Zhang, W. Jia, and X.-J. Liu, Universal topological quench dynamics for \mathbb{Z}_2 topological phases, *Sci. Bull.* **67**, 1236 (2022).
- [77] L. Zhou and J. Gong, Non-Hermitian Floquet topological phases with arbitrarily many real-quasienergy edge states, *Phys. Rev. B* **98**, 205417 (2018).
- [78] B. Zhu, Y. Ke, H. Zhong, and C. Lee, Dynamic winding number for exploring band topology, *Phys. Rev. Research* **2**, 023043 (2020).
- [79] L. Li, W. Zhu, and J. Gong, Direct dynamical characterization of higher-order topological phases with nested band inversion surfaces, *Sci. Bull.* **66**, 1502 (2021).
- [80] J. Niu, T. Yan, Y. Zhou, Z. Tao, X. Li, W. Liu, L. Zhang, H. Jia, S. Liu, Z. Yan, Y. Chen, and D. Yu, Simulation of higher-order topological phases and related topological phase transitions in a superconducting qubit, *Sci. Bull.* **66**, 1168 (2021).
- [81] Z. Lei, Y. Deng, and L. Li, Topological classification of higher-order topological phases with nested band inversion surfaces, *Phys. Rev. B* **106**, 245105 (2022).
- [82] W. Jia, X.-C. Zhou, L. Zhang, L. Zhang, and X.-J. Liu, Unified characterization for higher-order topological phase transitions, *Phys. Rev. Res.* **5**, L022032 (2023).
- [83] W. Sun, C.-R. Yi, B.-Z. Wang, W.-W. Zhang, B. C. Sanders, X.-T. Xu, Z.-Y. Wang, J. Schmiedmayer, Y. Deng, X.-J. Liu, S. Chen, and J.-W. Pan, Uncover Topology by Quantum Quench Dynamics, *Phys. Rev. Lett.* **121**, 250403 (2018).
- [84] C.-R. Yi, L. Zhang, L. Zhang, R.-H. Jiao, X.-C. Cheng, Z.-Y. Wang, X.-T. Xu, W. Sun, X.-J. Liu, S. Chen, and J.-W. Pan, Observing Topological Charges and Dynamical Bulk-Surface Correspondence with Ultracold Atoms, *Phys. Rev. Lett.* **123**, 190603 (2019).
- [85] B. Song, C. He, S. Niu, L. Zhang, Z. Ren, X.-J. Liu, and G.-B. Jo, Observation of nodal-line semimetal with ultracold fermions in an optical lattice, *Nat. Phys.* **15**, 911 (2019).
- [86] Y. Wang, W. Ji, Z. Chai, Y. Guo, M. Wang, X. Ye, P. Yu, L. Zhang, X. Qin, P. Wang, F. Shi, X. Rong, D. Lu, X.-J. Liu, and J. Du, Experimental observation of dynamical bulk-surface correspondence in momentum space for topological phases, *Phys. Rev. A* **100**, 052328 (2019).
- [87] W. Ji, L. Zhang, M. Wang, L. Zhang, Y. Guo, Z. Chai, X. Rong, F. Shi, X.-J. Liu, Y. Wang, and J. Du, Quantum Simulation for Three-Dimensional Chiral Topological Insulator, *Phys. Rev. Lett.* **125**, 020504 (2020).
- [88] T. Xin, Y. Li, Y. ang Fan, X. Zhu, Y. Zhang, X. Nie, J. Li, Q. Liu, and D. Lu, Quantum Phases of Three-Dimensional Chiral Topological Insulators on a Spin Quantum Simulator, *Phys. Rev. Lett.* **125**, 090502 (2020).
- [89] Z.-Y. Wang, X.-C. Cheng, B.-Z. Wang, J.-Y. Zhang, Y.-H. Lu, C.-R. Yi, S. Niu, Y. Deng, X.-J. Liu, S. Chen, and J.-W. Pan, Realization of an ideal Weyl semimetal band in a quantum gas with 3D spin-orbit coupling, *Science* **372**, 271 (2021).
- [90] M.-C. Liang, Y.-D. Wei, L. Zhang, X.-J. Wang, H. Zhang, W.-W. Wang, W. Qi, X.-J. Liu, and X. Zhang, Realization of Qi-Wu-Zhang model in spin-orbit-coupled ultracold fermions, *Phys. Rev. Res.* **5**, L012006 (2023).
- [91] D. Yu, B. Peng, X. Chen, X.-J. Liu, and L. Yuan, Topological holographic quench dynamics in a synthetic frequency dimension, *Light Sci. Appl.* **10**, 209 (2021).
- [92] B. Chen, S. Li, X. Hou, F. Ge, F. Zhou, P. Qian, F. Mei, S. Jia, N. Xu, and H. Shen, Digital quantum simulation of Floquet topological phases with a solid-state quantum simulator, *Photonics Res.* **9**, 81 (2020).
- [93] J.-Y. Zhang, C.-R. Yi, L. Zhang, R.-H. Jiao, K.-Y. Shi, H. Yuan, W. Zhang, X.-J. Liu, S. Chen, and J.-W. Pan, Tuning Anomalous Floquet Topological Bands with Ultracold Atoms, *Phys. Rev. Lett.* **130**, 043201 (2023).
- [94] For the 2D parent integer phase of a 1D class D \mathbb{Z}_2 static Hamiltonian H_s , the n -th order BISs with n vanishing Hamiltonian components are of dimensionality $(2 - n)$. Hence the 0D highest-order BISs for H_s are denoted as 2-BISs.
- [95] A. Eckardt and E. Anisimovas, High-frequency approximation for periodically driven quantum systems from a Floquet-space perspective, *New J. Phys.* **17**, 093039 (2015).
- [96] Near the BISs, we can expand the Floquet Hamiltonian coefficients in terms of k_\perp as $h_{F,z}(k) \approx k_\perp$ and $h_{F,i}(k) \approx h_{F,i|2\text{-BIS}} + \mathcal{O}(k_\perp)$ for $i = x, y$. Then the dynamical field is given by $g_i \propto \lim_{k_\perp \rightarrow 0} (1/2k_\perp) \{ (2k_\perp)[h_{F,i} + \mathcal{O}(k_\perp)] / [|\mathbf{h}_F|^2 + \mathcal{O}(k_\perp)] \} = h_{F,i} / |\mathbf{h}_F|^2$.
- [97] The d D first (second) descendant \mathbb{Z}_2 topological phases can be derived as lower-dimensional descendants of the d' D parent Z topological phases with dimensionality being reduced by 1 (or 2); see Refs. [14, 98].
- [98] X.-L. Qi, T. L. Hughes, and S.-C. Zhang, Topological field theory of time-reversal invariant insulators, *Phys. Rev. B* **78**, 195424 (2008).
- [99] H. M. Price, O. Zilberberg, T. Ozawa, I. Carusotto, and N. Goldman, Four-Dimensional Quantum Hall Effect with Ultracold Atoms, *Phys. Rev. Lett.* **115**, 195303 (2015).
- [100] T. Ozawa, H. M. Price, N. Goldman, O. Zilberberg, and I. Carusotto, Synthetic dimensions in integrated photonics: From optical isolation to four-dimensional quantum Hall physics, *Phys. Rev. A* **93**, 043827 (2016).
- [101] L. Yuan, Q. Lin, M. Xiao, and S. Fan, Synthetic dimension in photonics, *Optica* **5**, 1396 (2018).
- [102] T. Morimoto, H. C. Po, and A. Vishwanath, Floquet topological phases protected by time glide symmetry, *Phys. Rev. B* **95**, 195155 (2017).
- [103] S. Xu and C. Wu, Space-Time Crystal and Space-Time Group, *Phys. Rev. Lett.* **120**, 096401 (2018).
- [104] J. Yu, R.-X. Zhang, and Z.-D. Song, Dynamical symmetry indicators for Floquet crystals, *Nat. Commun.* **12**, 5985 (2021).
- [105] B. A. Bernevig and T. L. Hughes, *Topological Insulators and Topological Superconductors* (Princeton University Press, 2013).